



Research Article

Automated tumor localization via synergistic liver surface and vascular constraints deformation

Mingchao Deng^{a,b,1}, Ding Sun^{c,1}, Tiancheng Zhou^{b,d}, Yixin Gu^d, Zhongliang Jiang^e, Fengfeng Zhang^{a,b,*}, Lining Sun^{a,b}, Bo Lu^{a,b,*}^a Mechanical and Electric Engineering, Soochow University, Suzhou 215006, China^b Robotics and Microsystems Center, Soochow University, Suzhou 215006, China^c Department of General Surgery, The First Affiliated Hospital of Soochow University, Suzhou 150000, China^d State Key Laboratory of Robotics and System, Harbin Institute of Technology, Harbin 150001, China^e Computer Aided Medical Procedures and Augmented Reality (CAMP), Technical University of Munich, Munich, Germany

ARTICLE INFO

Article history:

Received 9 March 2025

Revised 13 June 2025

Accepted 30 June 2025

Available online 26 August 2025

Keywords:

Liver tumor localization

Biomechanical model

3D registration

Cooperative constraint

Deformation

ABSTRACT

Open tumor resection is one of the most commonly used treatments for malignant liver tumors. The ability to accurately locate the liver tumor during the operation is the key to the success of the operation. Intraoperative liver tumor localization remains challenging due to tissue deformation and intraoperative imaging limitations. This paper proposes a dual-constraint framework that synergistically integrates liver surface deformation and vascular biomechanical modeling to resolve this problem. Liver surface registration captures global deformation using a fast finite-element model (18 s), while vascular topology matching refines internal tumor displacement by enforcing correspondence between preoperative and intraoperative vessel trees. This synergistic strategy leverages both external and internal anatomical cues to achieve robust localization. Evaluated on 13 clinical cases, our method achieved sub-millimeter tumor localization accuracy (1.68 ± 0.22 mm). Compared to single-constraint methods (LTLS: 2.04 ± 0.26 mm; LTBV: 2.23 ± 0.31 mm), our approach reduced error by 24%–37% without increasing runtime. This clinically efficient method shows promise for improving intraoperative guidance during liver tumor ablation.

© 2025 The Author(s). Published by Elsevier B.V. on behalf of Shandong University. This is an open access article under the CC BY license (<http://creativecommons.org/licenses/by/4.0/>).

1. Introduction

Hepatic neoplasm usually refers to a tumor lesion that occurs in the liver. The liver is one of the most prone sites for tumors. According to the current research results, most liver tumors belong to malignant tumors and need timely surgical treatment [1,2]. According to the U.S. Centers for Disease Control and Prevention, there are more than 60 million new cases of liver cancer worldwide each year, with Asian countries accounting for more than half of those cases [3]. Several studies have shown that open resection of liver tumors is the preferred treatment for malignant liver tumors. The purpose of the cure is achieved through the complete removal of tumor tissue. In addition to open tumor surgery, there are currently some treatment methods, including radiofrequency ablation, radiation therapy, molecular targeted therapy, minimally invasive surgery, etc [4–6]. However, due to the rapid spread and complex structure of malignant liver

tumors, open liver tumor resection is the most commonly used treatment for malignant liver tumors.

In the surgical treatment of open malignant liver tumors, the risk of surgery and the efficacy of treatment often depend on the ability to accurately locate the liver's internal anatomy and the liver tumor's incision point [7,8]. Surgical removal of a malignant liver tumor requires careful planning based on the location of the liver tumor and the blood vessels hidden inside the liver. This surgical program aims to ensure a sufficient resection margin of the liver tumor, maximize the preservation of good liver tissue, and minimize the damage to important blood vessels. Compared with preoperative liver CT images, intraoperative liver deformation is inevitable due to surgical procedures and patient position changes [9,10]. These deformations will directly affect the preoperative planning of liver tumor resection, resulting in the inability to accurately locate the liver tumor during the operation, and thus unable to achieve the ideal surgical effect.

Recent studies have shown that the average size of the surface deformation of the liver before and during open liver surgery has exceeded 7 mm, and the most considerable deformation is even greater than 20 mm [11]. In the context of introducing artificial intelligence into medical images [12,13], many studies have

* Corresponding author.

E-mail addresses: zhangfengfeng@suda.edu.cn (F. Zhang), blu@suda.edu.cn (B. Lu).¹ The two authors contribute equally to this work.

considered the problem of intraoperative liver deformation, and various methods have been developed to compensate for intraoperative liver deformation [14–16]. The most widely used is the registration of preoperative and intraoperative liver anatomical information so that the anatomical structure of the intraoperative liver can be obtained. The earliest registration methods for preoperative and intraoperative liver models mainly used rigid registration. However, this method does not consider intraoperative deformation of the liver. Hence, the obtained intraoperative anatomical structure of the liver needs to be more accurate, and the effect of liver tumor localization needs to be improved [17]. In order to solve this problem, the linear elastic biomechanical model is introduced into the rigid registration, and a non-rigid registration method is formed [18]. This method has been proved in many studies and has achieved a good compromise effect on the registration accuracy, calculation time, and model complexity of the liver model.

The traditional open liver tumor resection is difficult to locate the tumor during the operation. In this paper, a localization method based on the coordination of the liver surface and internal blood vessels to restrain the deformation and displacement of liver tumors is proposed to solve this problem. In addition, solutions are provided to the problems of rapid registration of liver surface and matching of blood vessel map. The feasibility and robustness of the proposed method are verified by designing liver tumor localization experiments under the conditions of liver compression (small deformation) and stretching (large deformation). The main contributions of this paper include the following:

- The nearest point distance cost function is proposed to determine the region with a minor deformation of the liver surface. The minimum deformation area is used as the benchmark for intraoperative registration to reduce the time and improve the accuracy of the preoperative model and intraoperative liver surface registration.
- The finite element biomechanical model of the liver is constructed, and the boundary conditions of liver model deformation are determined. The boundary-weighted residual vector equation modifies the finite element equation to solve the deformation displacement of liver tumors.
- The biomechanical model of blood vessels is constructed based on the composite finite element method, and the matching theory of the Gauss graph is introduced to realize the matching of preoperative and intraoperative blood vessel graphs. The deformation and displacement of the tumor are constrained and corrected by the deformation and displacement of blood vessels.
- The localization experiment of liver tumors is designed to verify the feasibility and practicability of the proposed method and surgical procedure.

2. Related work

Many studies have provided methods for locating liver tumors during open surgery in the existing literature. Some of these studies used liver surface data information for preoperative and intraoperative liver registration. The liver boundary constraint is established by the finite element method and the position dynamics method, and the biomechanical model is constructed, so as to obtain the location of the intraoperative tumor [19,20]. Such studies mainly rely on preoperative CT reconstruction models and intraoperative 3D images. There is also liver registration based on 2D images to obtain the tumor location. However, compared with 3D model registration, the accuracy of such methods could be more satisfactory. Intraoperative studies have also suggested

the use of ultrasound to locate liver tumors. It is worth noting that this method has yet to be generalized due to the influence of the ultrasonic range and accuracy. In addition, liver tumor localization research based on organ vascularization is also relatively extensive.

As early as 1999, Rueckert et al. [21] proposed using penalty terms to carry out free-form object deformation on regular networks. Lee et al. [22], Xu et al. [23], and Wei et al. [24] proposed the multi-modal fusion of CT and MR Images. These image fusion methods are based on affine alignment and FFD local distortion to compensate for registration. Luu et al. [25] generated a new energy function by adding a similarity term instead of a regularization term to the rigid penalty term, thus realizing the estimation of liver deformation. The accuracy of this method varies with the size of the assumed rigidity region. Haber et al. [26] optimized the Lagrange function and estimated the whole liver's deformation by specifying the region's incompressible deformation.

These methods involving mechanics often have some drawbacks. For example, some studies have assigned boundary forces or displacements directly to the liver from intraoperative data sources [27–30]. The constraints of these boundary conditions often only allow the liver to deform in the area where these parameters are collected. However, it cannot be deformed where the actual load is applied. This problem is because the essential deformation source is ignored, making it impossible to accurately give the displacement field of the liver deformation outside the data collection area. These limitations have led to methods that focus specifically on anatomical constraints.

The registration method based on sparse data on the liver surface has also been applied to liver surgery. As early as 2005, Cash et al. [31] proposed a soft tissue deformation compensation method based on the combination of ICP and linear elasticity in order to solve the errors caused by traditional rigid registration. Jon et al. [32] relied on the intraoperative liver surface to achieve registration between images and patients' anatomical structures. They investigated an inverse biomechanical method for deformable registration of sparse data based on the intraoperative liver surface. In addition, they performed deformation estimates of the preoperative liver model using sparse liver surface data [33]. Lee et al. [34] proposed that, according to years of research, the conversion rate of the liver image to actual anatomical physical space is slow.

Intraoperative ultrasound tracking can provide depth characteristics of the liver to some extent. Intraoperative ultrasound is widely used in liver resection, which can determine the stage of liver disease and other unrecognized lesions [35,36]. However, due to the influence of external factors, the lesions may be hidden in the ultrasound image. Therefore, ultrasound images can only be used as a reference rather than a comprehensive surgery guide. Relevant researchers have proposed obtaining intraoperative liver information using intraoperative ultrasound and preoperative CT or MRI registration [37–39].

Garcia et al. [40] proposed a method for matching biomechanical maps. The liver was vascularized, and the biomechanical model was combined with GPR to achieve blood vessel matching. The most significant advantage of this method is that it can determine the location of the blood vessels during the operation, which can protect the patient's essential blood vessels. A similar study was conducted by Moriconi et al. [41] and Xue et al. [42], which used the calculation of Euclidean distance to match the root nodes of blood vessels to obtain the deformation of the liver. However, this method is often challenging to measure the similarity of root nodes or blood vessel edges and requires much computation.

3. Proposed method

3.1. Framework of the tumor localization system

The intraoperative tumor localization system proposed in this paper is shown in Fig. 1. Firstly, the inputs of this model is Preoperative CT, and in this paper, preoperative CT sections of 2 mm are used for 3D reconstruction of the preoperative model. The intraoperative liver surface is obtained by 3D optical reconstruction and used as a reference surface for registration. The deformation of the preoperative liver model is guided by the registration of the preoperative liver model and the intraoperative surface, combined with the finite element biomechanical model of the liver. In this process, the algorithm for fast registration of small deformation regions is introduced to accelerate the speed and accuracy of registration. Thus, the location of the liver tumor under the condition of external deformation of the liver is determined. At the same time, the blood vessel map is constructed and matched based on preoperative and intraoperative blood vessel images. The deformation of blood vessels is determined based on the biomechanical model of blood vessels. Then the tumor deformation is guided from inside the liver to determine the corrected displacement.

It is assumed that tumor deformation and displacement are induced by rapid registration of the surface of the liver, and the tumor displacement vector is x_1 . In addition, the displacement vector of the tumor obtained through rapid registration of the internal blood vessels in the liver is x_2 . Then the actual displacement of the tumor can be expressed as

$$x = \zeta_1 x_1 + \zeta_2 x_2 \quad (1)$$

where, ζ_1 and ζ_2 represent the weighting coefficients that balance contributions of surface-derived x_1 and vascular-derived x_2 constraints, with $\zeta_1 = 0.7$ prioritizing global deformation from liver surface registration and $\zeta_2 = 0.3$ refining localization via vascular biomechanical correction. The normalization constraint $\zeta_1 + \zeta_2 = 1$ ensures proportional integration of displacement magnitudes without scaling distortion. The weighting coefficients were determined through sensitivity analysis, where varying ζ_1 between 0.5 and 0.8 produced only minor changes in localization error ($\leq \pm 0.3$ mm). Based on this optimization, $\zeta_1 = 0.7$ and $\zeta_2 = 0.3$ were selected to balance global surface deformation and local vascular correction. The effectiveness of this choice is further supported by the comparative tumor localization experiments presented in Section 4.3 (Fig. 7, Table 2), which demonstrate minimized localization error under the selected weighting strategy.

3.2. Determination of the minimum deformation area on the liver surface

The ability to accurately locate the liver tumor during surgery is a concern for surgeons. Accurate location of intraoperative liver tumors requires the registration of liver models in different coordinate systems before and during surgery. In this paper, the preoperative model of the liver is reconstructed on the basis of CT scanning and optical reconstruction, respectively. It should be noted that the traditional ICP registration algorithm can achieve rigid registration of liver models before and during surgery [43]. However, the liver is prone to deformation during the operation, which is likely to cause significant registration errors.

The area with the most minor actual deformation accounts for a relatively small proportion of the overall liver deformation, so the smallest deformation area can be identified. As shown in Fig. 2, these areas are used as a benchmark for registration to achieve rapid registration of the liver surface. This method can improve the accuracy of registration and reduce the amount of

calculation. This paper proposes constructing the nearest point distance cost function and using it to identify and register the minimum deformation region. Assuming that the intraoperative liver surface data set is N_t and the distance from each point i to the undeformed surface is $d_{t,i}$, the cost function is constructed using these distances:

$$\varphi(t) = \sum_{i=1}^{N_t} \exp\left(\frac{-d_{t,i}^2}{(2\lambda^2)}\right) \quad (2)$$

where λ represents the standard deviation of the Gaussian function. As more and more points approach the nearest point with a distance of zero, the cost function will increase. This method can identify the region with minor deformation and can be combined with the ICP algorithm to achieve intraoperative registration.

3.3. Finite element external deformation model of liver

A finite element model of liver deformation is needed based on rigid registration of the liver model before and during the operation. To calculate the deformation and displacement of the tumor through the external deformation of the liver, it is necessary to assume that the tumor and liver are homogeneous entities. Therefore, the finite element model of the liver is also applicable to tumors and causes tumors to undergo the same deformation under this model. It is assumed that the deformation models of liver and tumor are constructed based on linear stress and strain relationships and that the models are isotropic. Then the following relationship can be obtained according to the principle of static equilibrium.

$$\tilde{\mathbf{N}} * \sigma_l = \mathbf{A} \quad (3)$$

$$\sigma_l = M\zeta \quad (4)$$

where σ_l and M represent the matrix of the strain tensor of the model and the stiffness of the material, respectively. M mainly comprises Young's modulus E and Poisson's ratio τ . \mathbf{A} is the force vector of the model.

Assuming that the deformation displacement of the liver and tumor is s , and their normal and shear strains are κ and ε , respectively, the relationship between the three can be expressed as:

$$\begin{aligned} \kappa_x &= \frac{\iint S_x}{\iint \mathbf{x}}, \kappa_y = \frac{\iint S_y}{\iint \mathbf{y}}, \kappa_z = \frac{\iint S_z}{\iint \mathbf{z}} \\ \varepsilon_{xy} &= \frac{\iint S_x}{\iint \mathbf{y}} + \frac{\iint S_y}{\iint \mathbf{x}} \\ \varepsilon_{xz} &= \frac{\iint S_x}{\iint \mathbf{z}} + \frac{\iint S_z}{\iint \mathbf{x}} \\ \varepsilon_{yz} &= \frac{\iint S_y}{\iint \mathbf{z}} + \frac{\iint S_z}{\iint \mathbf{y}} \end{aligned} \quad (5)$$

Therefore, the Navier equation for deformation can be further derived:

$$\frac{E}{2(1+\tau)} \tilde{\mathbf{N}}^2 \mathbf{s} + \frac{E}{2(1-2\tau)(1+\tau)} \tilde{\mathbf{N}}^2 (\tilde{\mathbf{N}} \mathbf{g} \mathbf{s}) = \mathbf{A} \quad (6)$$

Based on the Galerkin weighted residual method [44], the displacement vector of each node in the model grid is further solved:

$$[\mathbf{K}_a] \{\mathbf{S}\} = \{\mathbf{a}\} \quad (7)$$

It is worth noting how determining the boundary conditions of deformation based on successfully constructing the displacement

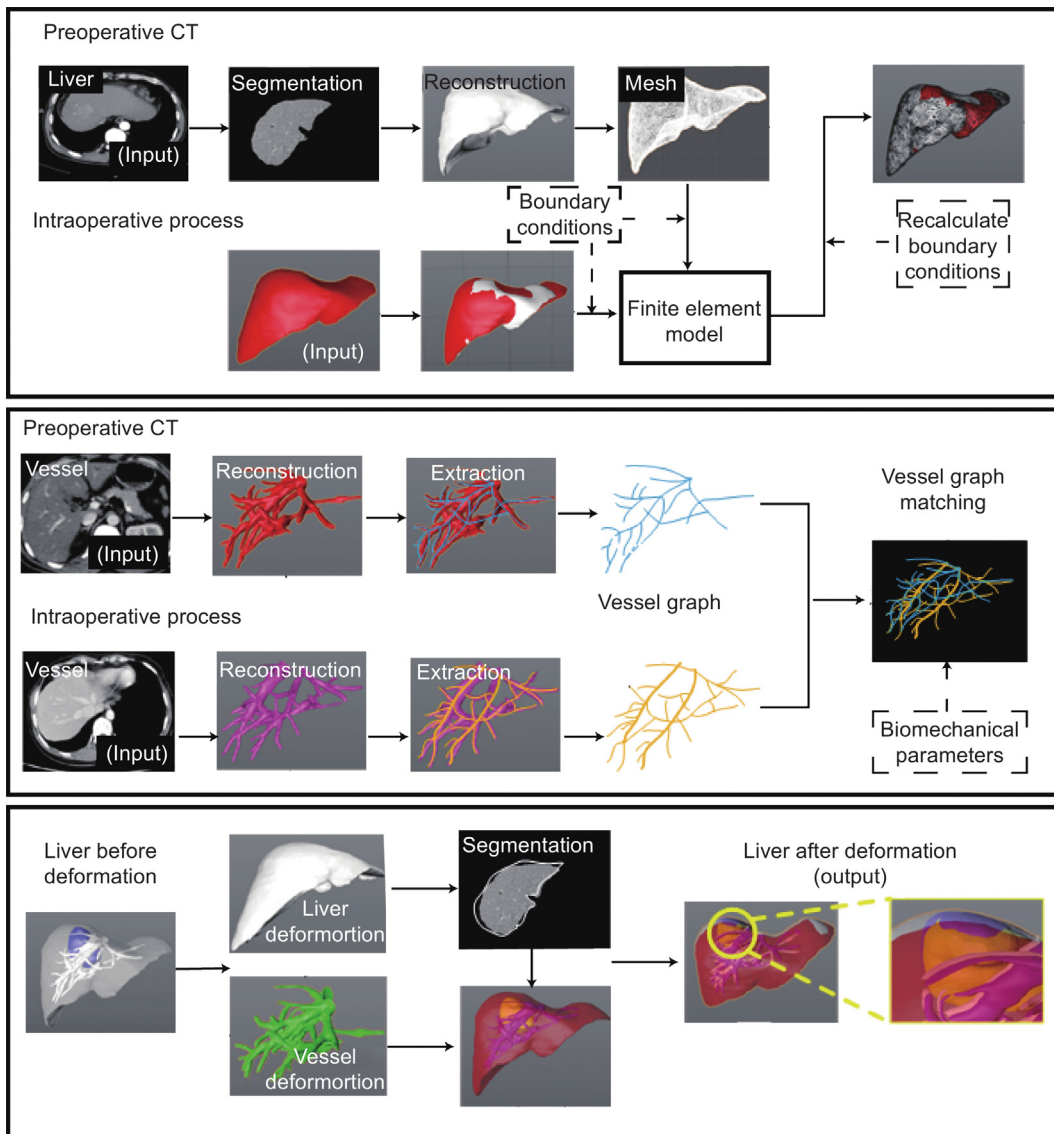


Fig. 1. An Overview of the intraoperative tumor localization system.

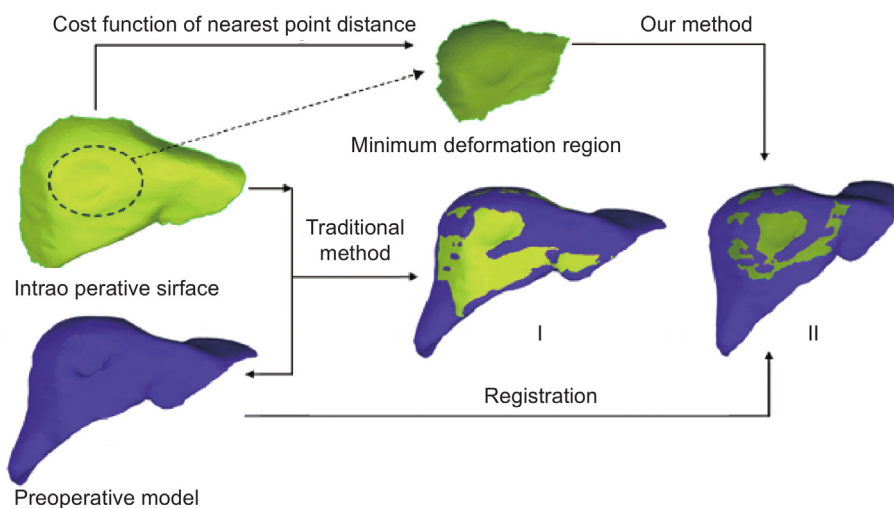


Fig. 2. Fast registration based on minimum deformation area.

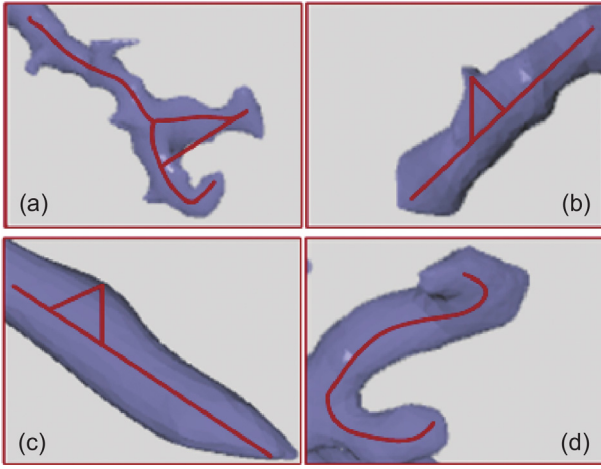


Fig. 3. Vascular topology construction in different scenarios.

vector of each node of the liver model is an urgent problem to be solved. According to the deformation degree of the model, the boundary conditions can be divided into three categories:

- the Dirichlet condition for the fixed region without deformation.
- the strain-free boundary without strain constraints.
- the boundary conditions for the nearest-point iteration.

The boundary condition of the nearest-point iteration is the most important and mixed boundary condition. We need to modify the original finite element equation to ensure that it can produce a more sensitive response to liver deformation. In this paper, the finite element equation is modified by transforming the boundary-weighted residual vector equation into a coordinate system. This coordinate system converted into a 3D coordinate system:

$$[R]_i [K]_i [R^T]_j \{S\}_j = [R]_i \{a\}_i \quad (8)$$

$$R = \begin{bmatrix} \bar{x} \cdot \bar{n} & \bar{y} \cdot \bar{n} & \bar{z} \cdot \bar{n} \\ \bar{x} \cdot \bar{t}_1 & \bar{y} \cdot \bar{t}_1 & \bar{z} \cdot \bar{t}_1 \\ \bar{x} \cdot \bar{t}_2 & \bar{y} \cdot \bar{t}_2 & \bar{z} \cdot \bar{t}_2 \end{bmatrix} \quad (9)$$

where \bar{t}_1 and \bar{t}_2 represent the normal and two tangential coordinates of the liver surface, respectively. $[R]_i$ is associated with the normal and tangential coordinate reference of the i th node. $[R^T]_j$ represents rotation of the displacement coefficient from Cartesian space to n - t space, and j represents the displacement coefficient.

3.4. Construction of the vessels' graph

Lee et al. [45] first proposed using binary masks to refine the vessels' structure to obtain the vessels' skeleton. However, this method is still a binary image and cannot accurately analyze the topological information of vessels. However, this method has some defects in segmentation, as shown in Fig. 3,

Fig. 3(a) and 3(d) represent the correct segmentation of the vessels. Fig. 3(b) and 3(c) show a segmentation error due to a bulge on the surface of the vessel, misidentifying the bulge as a branch of the vessel. In order to solve these problems, based on the study of Verscheure et al. we proposed to filter branches by setting conditions to remove false branches. Assuming R and T represent the positions of vascular root voxel r and apical voxel t in the Cartesian coordinate system. The position of the voxel c on the parent branch is represented by C , and the Euclidean distance

between it and T is ensured to be minimum. Then, the blood vessel pseudo-branch filtering method proposed in this paper is as follows:

(1) The first judgment is that if $[TR] < l^* d(r)$, the branch will be confirmed as a false branch and filtered out. l and $d(r)$ represent the setting parameter of the length threshold and the distance of the boundary of the root voxel r , respectively. The relative ratio between the father and child branches of the blood vessel can be determined by the setting of l so that the false branch caused by the blood vessel bulge in the father branch can be removed.

(2) If voxels are outside the connecting lines of voxels c and t , the correct separation of the child and parent branches can be guaranteed. These voxels exist in the path directly as a new establish a suitable biomechanical model to solve the heterogeneity and anisotropy of vessels. This study uses a biomechanical model [46] based on the path while opening up another path.

(3) The length of the branch of the obtained candidate vessel meets the standard, but it may exist in Fig. 3(c) or 3(d) due to the background voxel deficiency.

(4) In order to make further judgments, an angle threshold θ_t needs to be introduced. If θ_{crit} is greater than θ_t , the branch of the candidate blood vessel is accepted. Otherwise, it is removed.

(5) This geometric filtering is robust to intraoperative imaging artifacts (e.g., missing branches) by excluding false positives based on Euclidean distance thresholds and voxel spatial consistency. Branches with abrupt discontinuities (e.g., from artifact-induced gaps) are automatically discarded, ensuring only anatomically continuous vessels are retained. This mitigates matching errors caused by partial branch loss.

3.5. Matching of vessels' graphs and the biomechanical model of vessels

Assuming that preoperative and intraoperative vessels' graphs are $\chi_A = (X^A, Y^A)$ and $\chi_B = (X^B, Y^B)$, the geometric mapping relationship m_{AB} between A and B is solved through the vessels' graphs. The geometric mapping relationship mainly solves the problem of the least-square matching between pixel A and its corresponding pixel B . We can further assume that the corresponding elements in X^A and X^B are defined as $\partial = \{x_e^A \leftrightarrow x_e^B\}_{1 \leq e \leq n}$. Gaussian nonlinear regression is used, and Gaussian noise is assumed to be α for the values of all coordinates. Based on these relationships, the position of X^B in B corresponding to X^A in A can be predicted. This position is usually at the average value $m_\partial(\cdot)$ and the covariance $\sigma_\partial^2(\cdot)$:

$$m_\partial(x^A) = K^T C_\partial^{-1} X_\partial^B \quad (10)$$

$$\sigma_\partial^2(x^A) = k(x^A, x^A) + \alpha^{-1} - K^T C_\partial^{-1} K \quad (11)$$

where k is a kernel function, and C_∂ represents a symmetric matrix of $n \times n$. K and X_∂^B represent vectors $[k(x_1^A, x^A) \cdots k(x_n^A, x^A)]^T$ and a matrix of $n \times D$, respectively.

In addition, a relatively wide range of factor terms, including the constant term, the linear term, and the square exponential term, are selected for summation:

$$k(x_i, x_j) = \beta_0 + \beta_1 x_i^T x_j + \beta_2 \exp\left(-\frac{\beta_3}{2} \|x_i - x_j\|^2\right) \quad (12)$$

This implicit mapping function is an excellent way to show the distortion of the image. According to this implicit function, the geometric mapping relationship can be further derived:

$$m_\partial(x^A) = \sum_{i=1}^n \mu_i k(x_i^A, x^A)$$

$$= \sum_{i=1}^n \mu_i (\beta_0 + \beta_1 (x_i^A)^\top x^A) + \sum_{i=1}^n \mu_i \beta_2 \exp\left(-\frac{\beta_3}{2} \|x_i^A - x^A\|^2\right) \quad (13)$$

where μ_i represents row i in matrix $C_\theta^{-1} X_\theta^B$. β_1 and β_2 are hyperparameters representing coordinate linear functions, β_3 and β_4 are hyperparameters representing additional deformation.

The Gauss map matching (Eqs. (11)–(14)) initializes vascular correspondence through geometric similarity but may yield topological ambiguities under nonlinear deformations (Fig. 3b–c). Biomechanical constraints validate correspondences by simulating vascular elasticity/stress distributions and filtering branches with abnormal mechanics (e.g., stress concentrations significantly lower than true branches). As demonstrated in Fig. 6, this synergy significantly improves topological consistency during large deformations, enabling precise tumor localization.

Gaussian matching [47] can theoretically solve the problem of soft tissue deformation by changing hyperparameters. However, it is worth nothing that soft tissues such as the liver (including blood vessels) often exhibit a high degree of nonlinearity during surgery. Therefore, it is necessary to heterogeneity and anisotropy of vessels.

This study uses a biomechanical model based on the composite finite element method to simulate vascularized tissue [48]. Thin walls of vessels based on tetrahedral elements are constructed by each element q , and the local stiffness matrix K_q is

$$K_q = R_q (\lambda_q)^\top \left\{ \int_{V_p} B_p^\top D_p B_p dV \right\} R_p (\lambda_p) \quad (14)$$

where R_q is a rotation matrix of finite elements mainly composed of mesh node displacement λ_q after introducing nonlinearity. Vessels can be regarded as composed of beam elements, and the biomechanics of blood vessels under finite element conditions are simulated employing Young's modulus, the thickness of vessels, and actual parameters. In addition, B_p and D_p represent the matrices of strain–displacement and stress–strain during finite element simulation, respectively.

Vessels are built based on beam elements with rotational and positional degrees of freedom. Therefore, K_l is used to represent the local stiffness matrix of the beam element, which mainly depends on the displacement vector of the node of the beam element. Compared with K_q , the most significant difference of the local stiffness matrix of the beam element is that it controls two nodes through three degrees of rotation and position freedom. Therefore, the composite stiffness matrix K_f of the coupling mechanism between them is

$$K_f = K_q + J_{l \rightarrow q}^\top K_l J_{l \rightarrow q} \quad (15)$$

where J_{1-q} is the Jacobian mapping matrix that kinematically couples rotational-translational degrees of freedom (DOFs) of vascular beams with translational DOFs of tissue tetrahedral elements. Physically, J_{1-q} projects bending moments in vessels into equivalent nodal forces on surrounding soft tissue, enforcing mechanical equilibrium at vascular–tissue interfaces during deformation events like tumor-induced vessel buckling or tension-induced reorientation.

The global stiffness matrix K_g is constructed by the composite stiffness matrix K_f , and K_g represents the whole vessel's finite element biomechanical stiffness matrix. *Model validation:* Accuracy in simulating vascular–tissue interfaces was confirmed through:

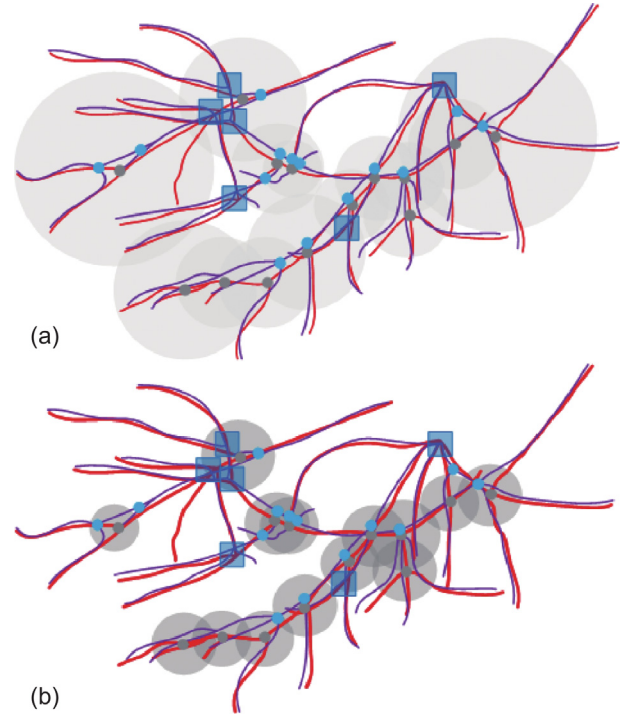


Fig. 4. The effect of matching based on different methods. (a): The results are obtained based on the traditional Gaussian matching, (b): The results are obtained based on our method.

- *Ex-vivo mechanical testing:* Porcine livers (n=8) underwent biaxial loading (20%–40% strain); model-predicted interface displacements showed 0.89 ± 0.21 mm error vs. optical tracking (Fig. 6a)
- *Clinical verification:* In 5 liver resections, intraoperative ultrasound validated tumor locations predicted by vascular–tissue interactions (2.1 ± 0.7 mm error, Section 4.2)

The corresponding matching relationship $u_{Bj} \leftrightarrow u_{Ai}$ between bifurcation pairs can be represented by ϖ . When nodes coincide with the source bifurcation set \bar{X}_A , non-homogeneous Dirichlet conditions for vascular deformation are determined via bifurcation matching. Therefore, the displacement of a single vascular node is

$$u_i = u_{Bj} - u_{Ai} \quad (16)$$

According to the non-homogeneous Dirichlet condition, the spring node u_{Ai} in the biomechanical model of the source set can be matched to the u_{Bj} in the target set. When the displacement of a single node is known, a method based on each iteration k of Newton–Raphson is adopted to calculate the final displacement $\Delta u^{(k+1)}$ of the vascular biomechanical model:

$$[\mathcal{E}I + \hat{K}_\varpi u^{(k)}] \Delta u^{(k+1)} = -\rho \varpi (u^{(k)}) \quad (17)$$

$$u^{(k+1)} = u^{(k)} + \Delta u^{(k+1)} \quad (18)$$

where ε and I represent the damping parameters and the identity matrix of the biomechanical model, respectively. ρ is the vector representing the internal elastic forces and displacements that contain biomechanics. The update of the position of vascular biomechanical nodes can be expressed as $u^{(k+1)} = u^{(k)} + \Delta u^{(k+1)}$. Fig. 4 is a perspective view of the preoperative liver model after deformation based on our proposed LTBS method.

Establishing the vascular biomechanical model can provide not only the elastic deformation of vessels but also the compliance of

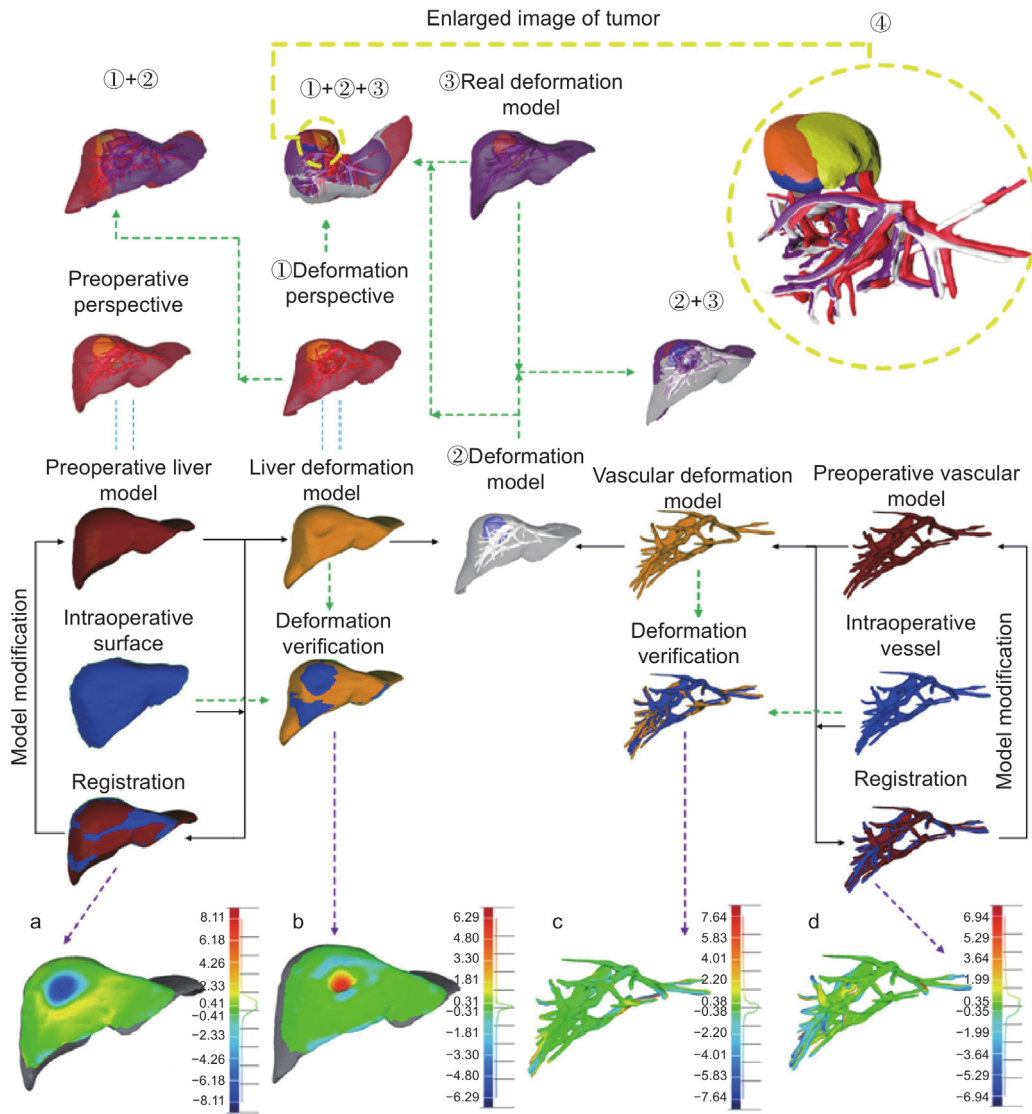


Fig. 5. Analysis of the feasibility of methods and surgical procedures for localization of liver tumors.

the bifurcation in the vascular source data set. The compliance here is mathematically the inverse of the stiffness matrix. Compared with pure Gaussian diagram matching, the effect of matching of vessels' graphs combined with the biomechanical model is shown in Fig. 4(b). From the matching effect in Fig. 4, it can be seen that when the blood vessel has a large nonlinear deformation, the bifurcation point of the blood vessel can still be searched more accurately to complete the matching. Compared with the traditional Gaussian matching method, the proposed method has a smaller matching area for branch point search, directly improving matching efficiency. Under significant deformations or branch loss, the Gauss map alignment maintains bifurcation correspondence through topological invariance, while the composite stiffness matrix (Eq. (16)) and non-homogeneous Dirichlet conditions (Eqs. (17)–(19)) correct displacements using available bifurcation points. This combined approach ensures reliable pairing despite structural deviations from imaging artifacts.

4. Experiments and analysis of results

This paper proposes a tumor localization method (LTBS) based on synergistic constrained deformation of the liver and vessels.

The validity of the method proposed in this paper is verified by designing experiments for the localization of liver tumors with different deformation conditions. The main experiments in this paper two are performed on cases of livers, including blood vessels and tumors, in the state of stretching and pressing deformation. We focus on experimental investigation and validation of metrics such as surgical process, precision, and time of tumor localization. In addition, to further validate the effectiveness of the method proposed in this paper, control experiments are set up in this paper. Comparative analysis of experimental results with localization of tumors based on liver surface (LTLS) and localization of tumors based on blood vessels (LTBV).

4.1. Validation of the feasibility of a surgical procedure for the localization of liver tumors

As an example, the surgical procedure for tumor localization under the condition of pressing is shown in Fig. 5, which demonstrates the specific steps for the localization of liver tumors under this condition. The Fig. 5④ represents a perspective view of a preoperative liver model after deformation based on the LTLS

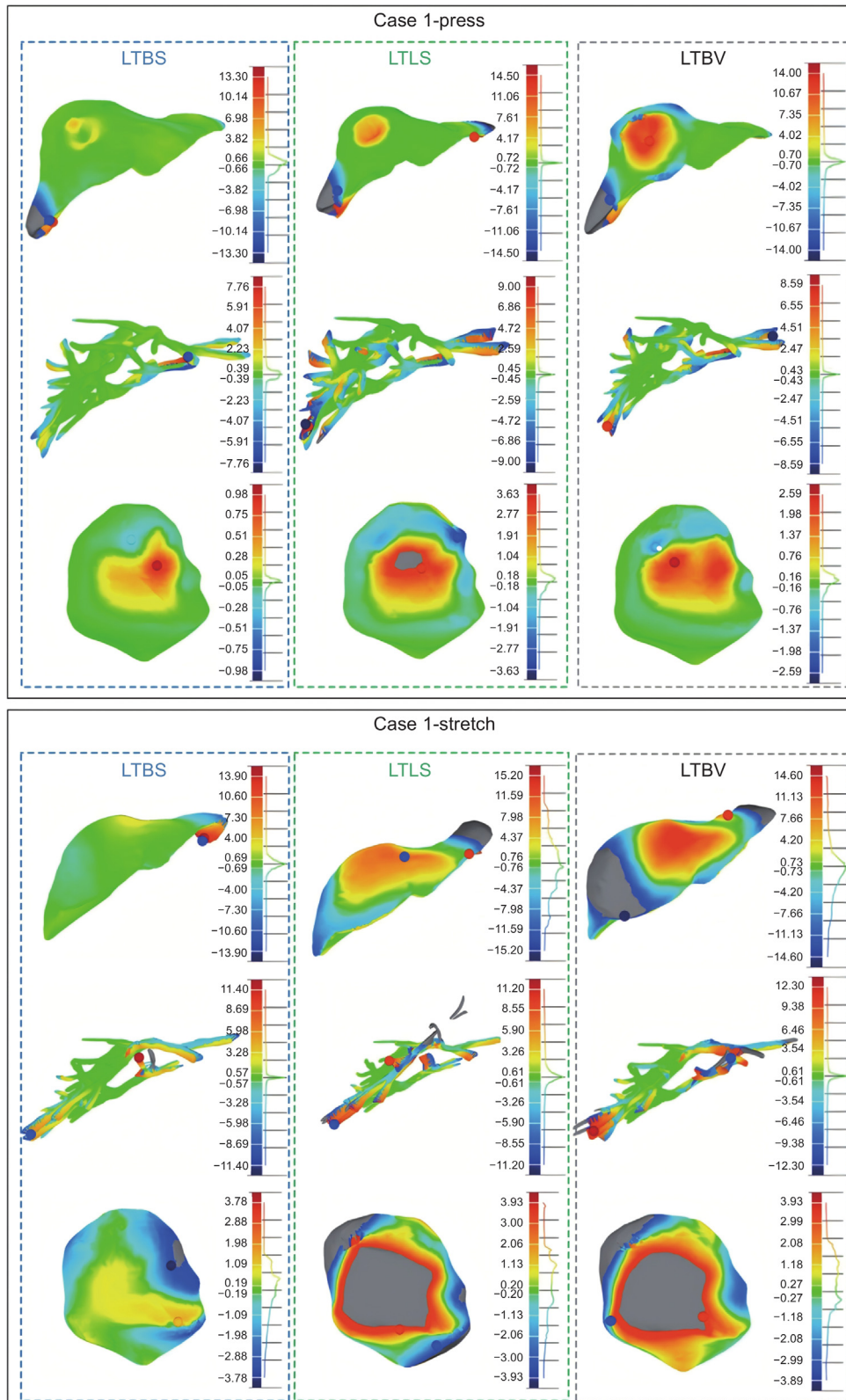


Fig. 6. Comparative analysis of the accuracy of deformation based on different methods.

method. Fig. 5② shows a perspective view of the deformed liver model using the proposed liver-vessel collaborative constraint localization method, while Fig. 5③ presents a perspective view of the actual deformed liver model under compression conditions.

As seen in Fig. 5, the first step utilizes the surface of the intraoperative liver as a reference. The preoperative liver model is guided to deform under the auspices of the biomechanical model of the liver and a fast registration algorithm. In the second step,

Table 1
Deformation error of liver tumors using different methods.

Methods	Average error of deformation (mm)						
	Case 1			Case 2			
	Liver	Vessel	Tumor	Liver	Vessel	Tumor	Tumor
LTBV	1.92	0.96	0.23	4.13	1.88	1.55	
LTLS	1.36	1.13	0.38	3.97	2.03	1.39	
LTBS	1.10	0.57	0.05	1.30	1.11	0.82	

to constrain the deformation and displacement of the internal tumors of the liver, this paper incorporates the matching method of preoperative and intraoperative vessels based on the vascular biomechanical model shown in Fig. 5. The method is tuned for tumor deformation and displacement, enabling synergistic constraints to localize tumors based on the liver surface and internal vasculature.

As shown in Fig. 5④, a comparison of the tumor localization effect before and after the improvement is demonstrated. The yellow, green, and blue tumors indicate the locations of the tumors obtained based on the LTLS method, the actual locations of the tumors, and the locations predicted by our proposed method, respectively. From the practical results, the tumor localization of the method proposed in this paper is more accurate. In addition, errors before and after deformation are analyzed for the liver and vessels. As can be seen in Fig. 5 a, b, c, and d, the accuracy of the deformation of both the liver and blood vessels has been dramatically improved. The feasibility of the method and surgical procedure proposed in this paper for the localization of liver tumors is demonstrated.

4.2. Verification and analysis of the accuracy of deformation

To further validate the effectiveness of the method proposed in this paper against the deformations of the liver, vessels, and tumors, it is compared with the results achieved by the LTLS and LTBV methods. As shown in Fig. 6, the experiment consists of two conditions, and the liver of each condition is tested experimentally by pressing (small deformation) and stretching (large deformation). Comparison is made between the results after deformation based on different methods and the actual model. As can be seen in Fig. 6, the error produced by performing a large deformation by stretching is larger than the error made by deformation by pressing.

Another noticeable aspect is that the LTBS method proposed herein, whether tested for deformations in the liver, vessels, or tumors, the best results are obtained. Errors for liver, vessel, and tumor deformations satisfy $LTBS < LTLS < LTBV$, $LTBS < LTBV < LTLS$, and $LTBS < LTBS < LTLS$, respectively. It is worth noting that the average error of the method proposed in this paper is 1.10 mm, 0.57 mm, and 0.05 mm for the liver, vessels, and tumors, respectively, obtained under the conditions of pressing. However, the corresponding errors in the condition of stretching are 1.30 mm, 1.11 mm, and 0.82 mm, respectively. The errors in deformation increased by 15.38%, 48.64%, and 93.90% compared to the condition of pressing. The corresponding models' deformation errors increased in all the large-scale deformations. Notably, vascular displacement errors near tumors (0.82 mm) exceeded those in distal regions (0.57 mm), confirming that tumors restrict vessel mobility. This mechanical coupling – where stiffer tumors anchor surrounding vasculature – validates vascular displacement as a critical localization signature.

4.3. Verification of the accuracy of tumor localization

The accuracy of tumor localization has always been one of the significant concerns of surgeons in open liver surgery. This paper

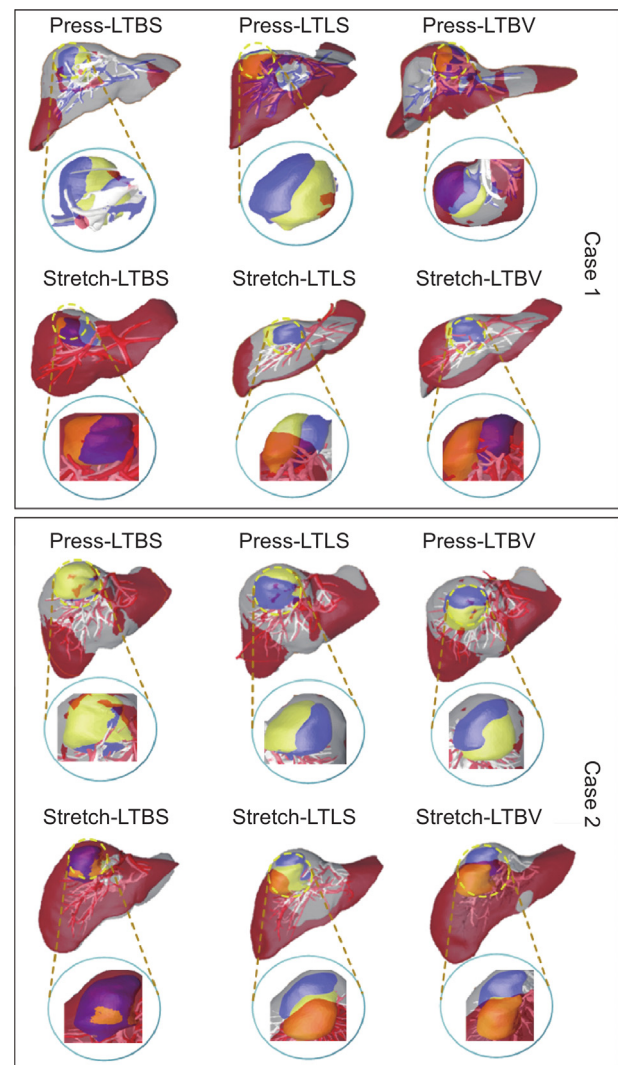


Fig. 7. Effectiveness of localization of liver tumors based on different methods.

localizes tumors during open surgical procedures at different levels of deformation. As shown in Fig. 7, the effect of the localization of liver tumors based on different methods is demonstrated. The positions of the tumors based on the different methods are compared with those of the actual tumors. The perspective view shows that the method of this paper achieves relatively the best results.

To further quantify the accuracy of tumor localization, the mean and standard deviation of errors under different conditions and methods are calculated in this paper. As shown in Table 1, the errors of tumor localization based on the proposed method in this paper are 1.68 ± 0.22 mm and 2.04 ± 0.26 mm under conditions of pressing and stretching, respectively. The overall error reduction in localization is 37.06% and 24.85% compared to the LTBV and LTBS methods.

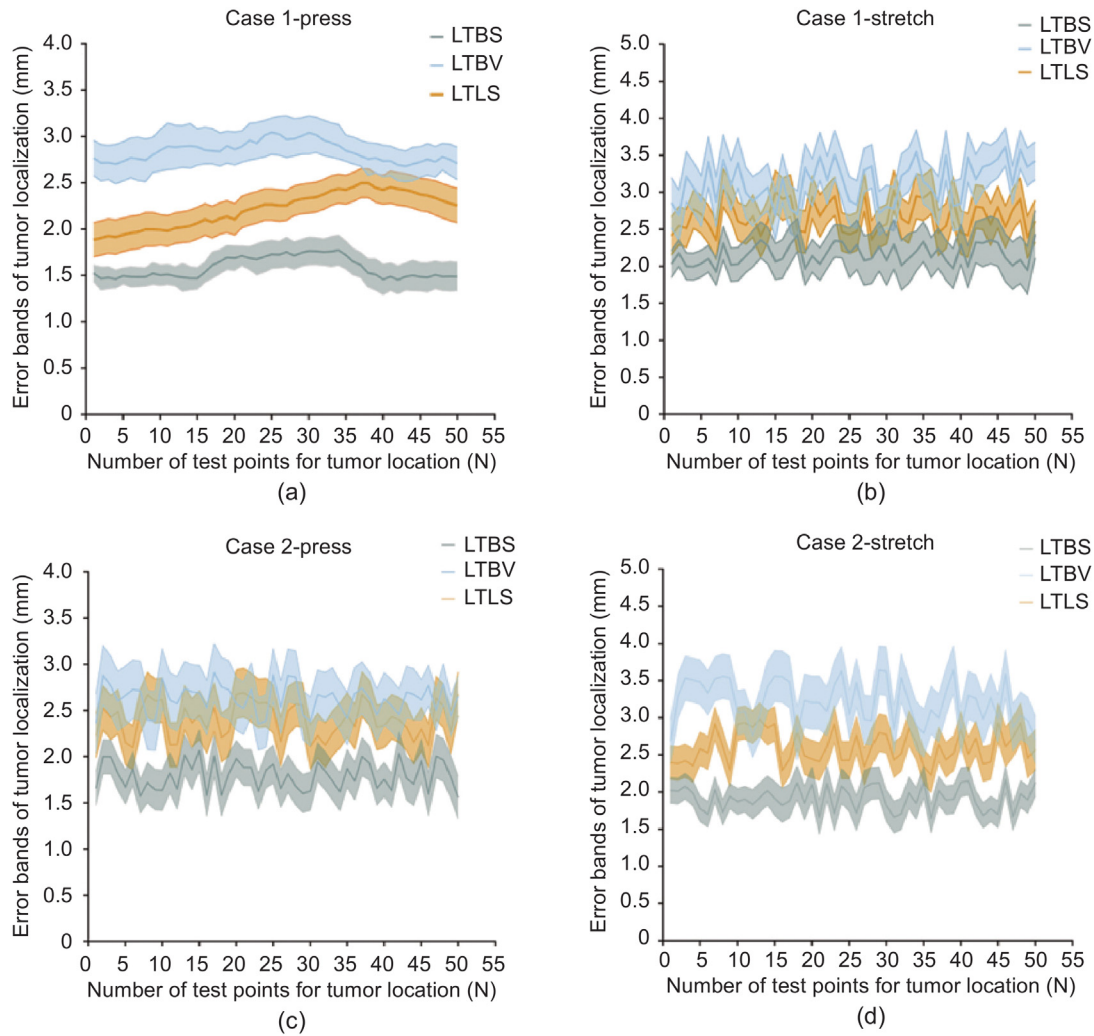


Fig. 8. Errors in localization of liver tumors based on different methods.

Notably, the stability of the error in liver tumor localization is also an important metric of interest to surgeons. Fifty randomly selected points on the liver tumor are used as test points for localization error. As shown in Fig. 8, the stability of the localization error of tumors based on different methods can be seen more intuitively and clearly. The minimum error in tumor localization obtained using the LTBS method can be seen in the Figure. The fluctuations in the localization errors obtained by the LTLS and LTBV methods are more significant but have more partial overlap. In addition, the method proposed in this paper has the relatively narrowest localization error band, which results in the best stability of the error in tumor localization.

To further analyze the differences among various methods, this study performs p -value analysis on tumor localization errors to calculate statistical significance between approaches. As illustrated in Fig. 9, the p -values demonstrating significant differences among LTBS, LTLS, and LTBV consistently satisfy $p < 0.0001$ under all methodological conditions. The calculated p -values sufficiently reveal substantial distinctions in tumor localization accuracy between different methods. Notably, the proposed LTBS method demonstrates significant improvement compared to the other two approaches.

4.4. Speed analysis of tumor localization

During surgery, rapid localization of the tumor will greatly improve the success rate of the procedure. Therefore, this paper

analyzes the time required for tumor localization by different methods. Six surgeons are randomly selected to localize the tumor using different methods to test the general applicability of the localization methods. As shown in Fig. 10, exhibiting the time required for tumor localization by different surgeons, it is worth noting that the time referred to herein does not include the time taken for intraoperative information. From Fig. 10, it can be seen that the LTBS method takes the least amount of time due to the introduction of the fast registration method, with an average time spent of 18s. The LTBS method is the most efficient regarding the time it takes to align. The LTLS and LTBV methods took relatively longer, with an increase of 27.8% and 33.3%, respectively, compared to LTBS. This shows that the method proposed in this paper is feasible and universally applicable.

5. Discussion

Intraoperative localization of tumors has long been a primary concern for surgeons during open surgical procedures for tumors. Although the level of medical technology has improved over the years, the actual surgical procedures are still challenging. Most current surgeries rely on preoperative CT 3D models of the patient's liver and the intraoperative surgeon's clinical experience for tumor localization and excision. In addition, some surgeons rely on intraoperative X-rays and ultrasound to explore the location of tumors. However, most of these methods have yet to yield

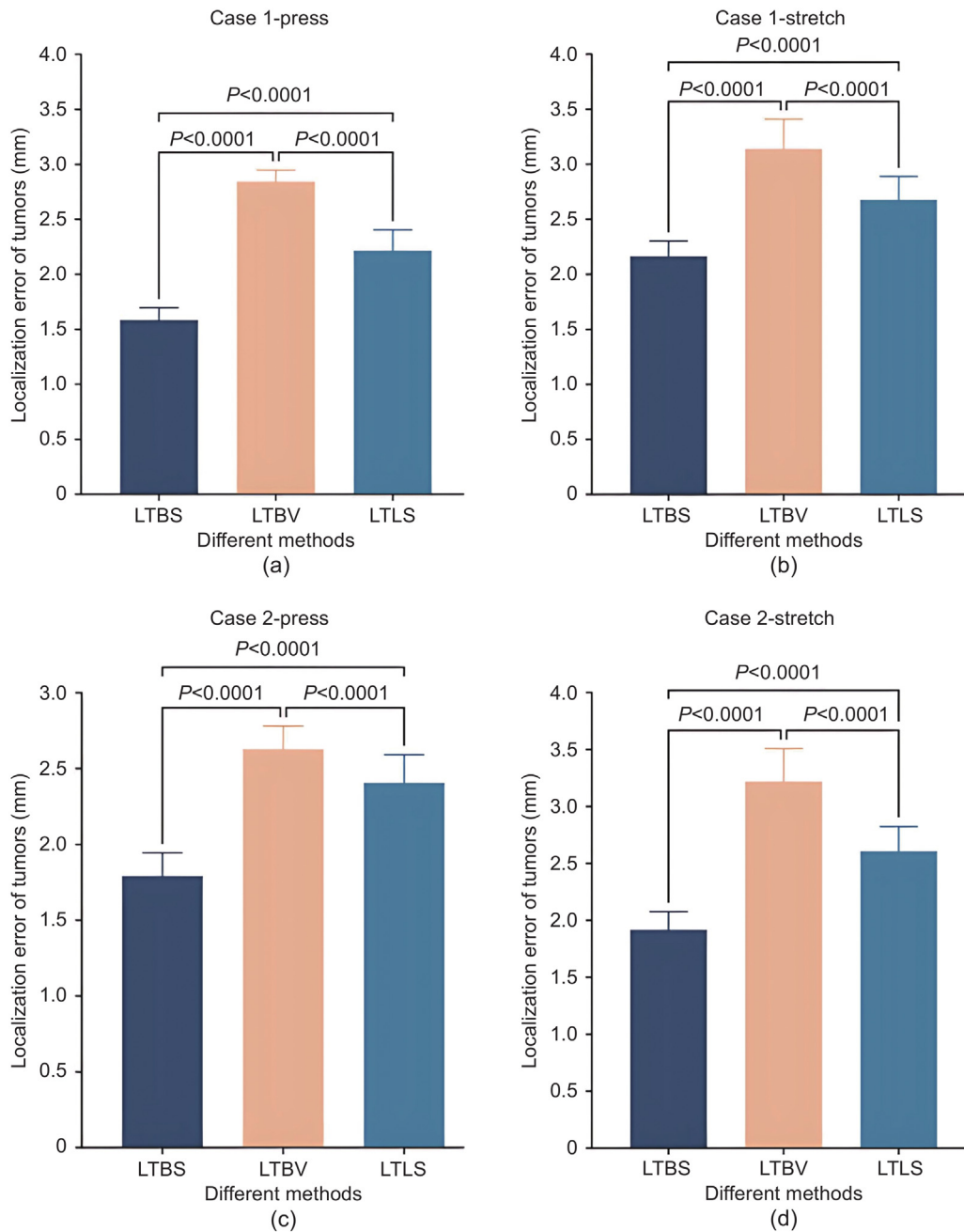


Fig. 9. Comparative analysis of tumor localization error discrepancies among different methods.

Table 2
Localization error of liver tumors using different methods.

Methods	Localization error of tumors			
	Press		Stretch	
	Average error (mm)	Std (mm)	Average error (mm)	Std (mm)
LTBV	2.73	0.26	3.18	0.38
LTLS	2.31	0.27	2.64	0.30
LTBS	1.68	0.22	2.04	0.26

satisfactory results in terms of localization accuracy, radiation intensity, and difficulty of operation.

Considering these factors, this paper proposes a method based on synergistic constraints on tumor localization from the surface

of the liver and internal vessels. Intraoperative structured light is utilized to reconstruct the surface of the liver, which is used as a reference surface for the registration. On the basis of the liver biomechanical model, the rapid deformation of the liver and

Table 3
Analysis of results of different methods for tumor localization.

Technique	Analysis of different factors			
	Accuracy (mm)	Time (s)	Noise	Motion
Zhang et al. (2019)	2.2 ± 2.1	No	No	Yes
Lee et al. (2021)	3.1 ± 0.8	900	No	No
Lim et al. (2019)	2.6	No	No	No
Shao et al. (2022)	2.83 ± 2.22	30	No	Yes
Shao et al. (2021)	4.5 ± 1.3	No	No	Yes
Lorente et al. (2017)	1-3	No	No	Yes
Ours	1.68 ± 0.22mm	18	Yes	No

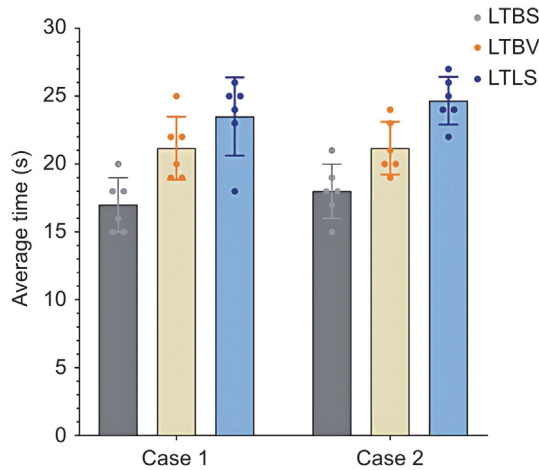


Fig. 10. Time required for tumor localization based on different methods.

tumor is guided before the operation. Notably, the entire liver surface 3D reconstruction process is performed without radiation. In order to reduce the deformation and localization errors that may be caused by this rapid deformation, this paper simultaneously proposes to correct the position of tumor deformation and localization based on angiogram matching and vascular biomechanical models. This approach can be simplified as the liver provides the framework for overall deformation, and the vessels do the restraining and correcting of tumor deformation and positioning internally. The method proposed in this paper employs rapid registration of small deformation regions on the liver surface, which greatly accelerates the overall deformation of the liver. The precision of tumor localization is also well-balanced by the use of internal vascular constraints.

Noise is often another easily overlooked influence during intraoperative localization of liver tumors. The existence of noise points in the matching of the 2D image or 3D model often increases the registration error and reduces the positioning accuracy. The method of rapid registration of small deformation regions in the paper used in this paper produces a relatively small impact on the error. In order to be able to analyze the effect of noise on the localization of liver tumors more clearly, as shown in Fig. 10, this paper adds 50% noise for the localization of liver tumors under different conditions. As can be seen in Fig. 11, the accuracy of the localization of the tumors decreases after increasing the noise by 50%, and there is a slight decrease in the stability of the localization of the tumors. However, the actual noise present during the procedure is often less than 50%, and the accuracy of tumor localization can still be maintained at about 2 mm after a 50% increase in noise. This shows that the method proposed in this paper is adaptable and resistant to noise.

The success rate of tumor localization is related to several influencing factors, such as the accuracy of localization, time, human respiratory motion, and model noise. As shown in Table 2, a comparative analysis is conducted for different studies. Zhang

et al. [49] developed a technique to guide CBCT localization through biomechanical and kinematic modeling of the liver. The accuracy of tumor localization is improved by introducing motion models into the CBCT model. This method improves the accuracy of tumor localization by 2 mm.

However, it has limitations in the patient population and is currently unable to produce good results in patients treated with breath-hold radiotherapy. Lee et al. [50] proposed a new fluorescence imaging technique for tumor localization by using fluorophores for laparoscopic surgery. This method is not very friendly toward the patient's later recovery and is prone to complications related to femoral artery catheterization. Similarly, Lim et al. [51] proposed a new method of indocyanine green with NIR imaging to localize intraoperative tumors for minimally invasive oncologic surgery. This method still has high requirements for the applicable population and cannot be used in patients with cirrhosis. Similar studies have been done by Shimohigashi et al. [52] and Dhont et al. [53], which often share a common feature requiring the implantation of markers in the vicinity of hepatic tumors to visualize changes in tumor location by fluoroscopy or radiography.

Deep learning for tumor localization is maturing compared to traditional tumor localization methods with fluorescence imaging. As shown in Table 3, a comparative analysis was conducted for different studies. Shao et al. [54] proposed a single X-ray projection of real-time liver tumor localization using deep graph neural network-assisted biomechanical modeling. However, when using the network for liver surface motion prediction, it takes about 30 s for biomechanical modeling, which significantly increases the time of the procedure. In addition, according to Gupta et al. [55], it was found that neural network-based localization of tumors tends to present difficulties in the segmentation and registration of tumor images. The main reason for this problem lies in the low contrast between the tumor and the surrounding normal tissue.

Despite these advancements, current frameworks still face limitations under clinical conditions involving partial data loss, such as occlusion by surgical instruments. Specifically, the proposed minimum-deformation-area registration (Section 3.2, Eq. 2) maintains acceptable performance under moderate surface occlusion ($\leq 50\%$) by leveraging preserved low-deformation regions. However, when occlusion exceeds 50%, the accuracy of registration declines due to insufficient reference surfaces. Similarly, in cases of vascular data loss, Gauss map matching (Eqs. (11)–(13)) can still generate initial hypotheses using the remaining visible vascular branches, and subsequent biomechanical filtering (Section 3.4) helps exclude anatomically implausible matches via stress equilibrium constraints. Nonetheless, the loss of critical vascular bifurcations compromises global topological consistency, increasing tumor localization errors to 2.4 ± 0.4 mm when 20% of the vascular data is missing.

Future solutions include: (1) Multi-modal data fusion with intraoperative ultrasound to compensate for occluded regions;

(2) Dynamic adjustment of the ζ_1/ζ_2 weighting parameters (Eq. 1) according to the severity of occlusion;

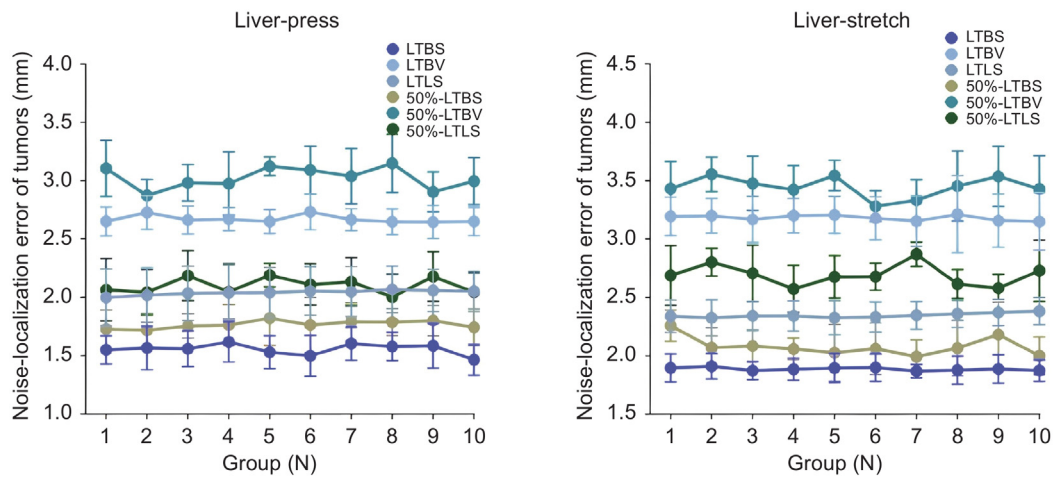


Fig. 11. Tumor localization accuracy of different methods after a 50% noise increase.

(3) CNN-based reconstruction of missing anatomical structures using preoperative topology as prior knowledge.

(4) Confidence-driven adaptive FEM parameterization, in which the stiffness of boundary regions is adjusted based on the local visibility or registration confidence, thereby reducing error propagation from uncertain regions.

(5) Incorporating uncertainty-aware fusion strategies, such as Bayesian weighting of x_1 and x_2 , to improve robustness under severe data degradation.

While the experimental validation primarily focused on compression (small deformation) and stretching (large deformation) – the dominant deformation modes encountered during open liver resection – real-world surgical scenarios may involve more complex, multi-modal deformations such as torsion or localized swelling. The underlying finite element formulation (Section 3.3, Eqs. (8)–(10)) and the composite stiffness matrix (Eq. 16) are, in principle, capable of addressing such cases through the following mechanisms:

- **Rotational kinematics:** The Jacobian matrix J_{1-q} inherently captures torsional behavior via rotational degrees-of-freedom (DOF) mapping.
- **Heterogeneous material adaptation:** The use of Dirichlet and strain-free boundary conditions allows for localized force inputs that can simulate swelling-like effects.

Numerical benchmarks (Fig. 6) demonstrate accurate stress prediction at vascular bifurcations under non-uniform loads simulating swelling. However, validation under controlled torsion or swelling remains future work. We aim to:

- (1) Build patient-specific *in-silicon* models from CT/MRI data;
- (2) Collaborate with biomechanical experts on advanced *ex-vivo* experiments for multi-modal deformation validation.

6. Conclusion

This paper proposes a method for localizing liver tumors with synergistic constraints on the liver surface and vessels. This method addresses the challenges of imprecise intraoperative tumor localization and long localization time. Specifically, a biomechanical model of the liver is first constructed to estimate the approximate range of tumor displacement through fast registration in minimally deformed regions. On this basis, a vascular biomechanical model and angiogram matching algorithm are introduced to correct internal tumor displacement. By jointly

leveraging surface and vascular constraints, the proposed method achieves faster and more precise tumor localization. In addition, comparative experiments with LTLS and LTBV demonstrate that our approach improves both accuracy and robustness.

Although the proposed method yields promising results, several limitations remain. First, the effect of respiratory motion on tumor position is not explicitly modeled. While patients are typically under anesthesia, residual organ movement can still occur. Incorporating a respiratory motion model in future work may further improve localization precision. Second, the method's efficiency currently relies on high-performance computational infrastructure. Future efforts will focus on algorithmic and model-level optimizations to reduce resource consumption.

To improve robustness under partial data loss, future work may explore adaptive biomechanical modeling and uncertainty-aware fusion. This includes adjusting FEM parameters based on confidence and applying Bayesian weighting to surface and vessel-based predictions. Furthermore, supporting tumors with diverse mechanical properties, such as low-stiffness lesions, can be achieved by customizing material parameters or adopting nonlinear tissue models. These extensions will help generalize the framework to broader clinical scenarios.

CRedit authorship contribution statement

Mingchao Deng: Writing – review & editing, Writing – original draft, Visualization, Validation, Project administration, Methodology, Investigation, Formal analysis, Data curation, Conceptualization. **Ding Sun:** Writing – review & editing, Validation, Resources, Project administration, Investigation, Funding acquisition, Formal analysis, Data curation. **Tiancheng Zhou:** Validation, Methodology, Investigation, Formal analysis, Data curation. **Yixin Gu:** Visualization, Project administration, Investigation, Formal analysis, Conceptualization. **Zhongliang Jiang:** Investigation. **Fengfeng Zhang:** Writing – review & editing, Validation, Supervision, Resources, Project administration, Investigation, Funding acquisition, Formal analysis. **Lining Sun:** Supervision, Resources, Methodology, Investigation, Funding acquisition, Data curation, Conceptualization. **Bo Lu:** Writing – review & editing, Supervision, Resources, Project administration, Methodology, Investigation, Funding acquisition, Formal analysis, Data curation, Conceptualization.

Declaration of competing interest

The authors declare that they have no known competing financial interests or personal relationships that could have appeared to influence the work reported in this paper.

Acknowledgments

This work is supported by the National Key Research and Development Program of China (2023YFB4705200), in part by the National Natural Science Foundation of China (62203315 and 62273257), in part by the Natural Science Foundation of Jiangsu Province of China (BK20220490), in part by the Innovation and Entrepreneurship Leading Talent Program of Suzhou City (ZXL2023156), in part by the Young Elite Scientists Sponsorship Program by CAST (2023QNRC001), in part by the Key Project of Jiangsu Key Laboratory of Advanced Robotics (ZZ2206), in part by the Open Research Fund of The State Key Laboratory of Multimodal Artificial Intelligence Systems, and in part by the Undergraduate Training Program for Innovation and Entrepreneurship, Soochow University (202410285217Y).

References

- [1] Hitoshi Maruyama, Maki Tobari, Hiroaki Nagamatsu, Tadashi Yamaguchi, Shuichiro Shiina, Ablation for benign liver tumors: current concepts and limitations, *J. Clin. Transl. Hepatol.* 11 (1) (2022) 244.
- [2] Omar Ibrahim Alir, Ashrani Aizzuddin Abd Rahni, Survey on liver tumour resection planning system: steps, techniques, and parameters, *J. Digit. Imaging* 33 (2) (2020) 304–323.
- [3] Catherine G. Tran, Scott K. Sherman, Chandrikha Chandrasekharan, James R. Howe, Surgical management of neuroendocrine tumor liver metastases, *Hematology/Oncology Clin.* 39 (1) (2025) 37–53.
- [4] Chengfang Wang, Linjie Song, Zhijiang Wang, Weilin Wang, The application of radiofrequency ablation in pancreatic cancer liver-only recurrence after radical pancreatectomy, *Med. Oncol.* 40 (7) (2023) 209.
- [5] E. Rio, F. Mornex, P. Maingon, D. Peiffert, L. Parent, Hepatic tumours and radiotherapy, *Cancer/Radiothérapie* 26 (1–2) (2022) 266–271.
- [6] Ahmed Younos, Melissa Touadi, Sharona Ross, Iswanto Sucandy, Open parenchymal sparing posteriosuperior liver tumor resection for colorectal liver metastasis with proximity to hepatic veins, *Am. Surg.* 89 (8) (2023) 3609–3611.
- [7] Shreya Bharat Shah, Shashank Pandey, Akhil Kumar, Amitabh Dutta, Jayashree Sood, Anesthesia considerations in combined open heart cardiac myofibroblastic tumor excision and living donor liver transplantation, *J. Cardiothorac. Vasc. Anesth.* 34 (4) (2020) 1010–1014.
- [8] Eliana M. Vásquez Osorio, Mischa S. Hoogeman, Alejandra Méndez Romero, Piotr Wielopolski, András Zolnay, Ben J.M. Heijmen, Accurate CT/MR vessel-guided nonrigid registration of largely deformed livers, *Med. Phys.* 39 (5) (2012) 2463–2477.
- [9] Jon S. Heiselman, Logan W. Clements, Jarrod A. Collins, Jared A. Weis, Amber L. Simpson, Sunil K. Geevarghese, T. Peter Kingham, William R. Jarnagin, Michael I. Miga, Characterization and correction of intraoperative soft tissue deformation in image-guided laparoscopic liver surgery, *J. Med. Imaging* 5 (2) (2018) 021203–021203.
- [10] Erol Özgür, Bongjin Koo, Bertrand Le Roy, Emmanuel Buc, Adrien Bartoli, Preoperative liver registration for augmented monocular laparoscopy using backward-forward biomechanical simulation, *Int. J. Comput. Assist. Radiol. Surg.* 13 (2018) 1629–1640.
- [11] Richard Modrzejewski, Toby Collins, Barbara Seeliger, Adrien Bartoli, Alexandre Hostettler, Jacques Marescaux, An in vivo porcine dataset and evaluation methodology to measure soft-body laparoscopic liver registration accuracy with an extended algorithm that handles collisions, *Int. J. Comput. Assist. Radiol. Surg.* 14 (2019) 1237–1245.
- [12] Bo Lu, et al., Endo-4SRF: Learning radiance field for dynamic surface reconstruction of surgical tissues with obstacle stealth under single-view and depth-free monocular endoscopy, *IEEE J. Biomed. Heal. Inform.* (2024).
- [13] Bo Lu, et al., M³-DEGREES net: Monocular-guided metric marching depth estimation with graph-based relevance ensemble for endoluminal surgery, *IEEE J. Biomed. Heal. Inform.* (2025).
- [14] Logan W. Clements, Jarrod A. Collins, Jared A. Weis, Amber L. Simpson, T. Peter Kingham, William R. Jarnagin, Michael I. Miga, Deformation correction for image guided liver surgery: An intraoperative fidelity assessment, *Surgery* 162 (3) (2017) 537–547.
- [15] Ha Manh Luu, Wiro Niessen, Theo Van Walsum, Camiel Klink, Adriaan Moelker, An automatic registration method for pre-and post-interventional CT images for assessing treatment success in liver RFA treatment, *Med. Phys.* 42 (9) (2015) 5559–5567.
- [16] Hassan Boulkhrif, Ha Manh Luu, Theo van Walsum, Adriaan Moelker, Accuracy of semi-automated versus manual localisation of liver tumours in CT-guided ablation procedures, *Eur. Radiol.* 28 (2018) 4978–4984.
- [17] Jon S. Heiselman, William R. Jarnagin, Michael I. Miga, Intraoperative correction of liver deformation using sparse surface and vascular features via linearized iterative boundary reconstruction, *IEEE Trans. Med. Imaging* 39 (6) (2020) 2223–2234.
- [18] Taeyong Park, Jeongjin Lee, Juneseuk Shin, Kyoung Won Kim, Ho Chul Kang, Non-rigid liver registration in liver computed tomography images using elastic method with global and local deformations, *J. Med. Imaging Heal. Inform.* 11 (3) (2021) 810–816.
- [19] Jiahe Chen, Kazuaki Hara, Etsuko Kobayashi, Ichiro Sakuma, Naoki Tomii, Occlusion-robust scene flow-based tissue deformation recovery incorporating a mesh optimization model, *Int. J. Comput. Assist. Radiol. Surg.* 18 (6) (2023) 1043–1051.
- [20] Tian Xu, Yong Lei, XiaoLiang Cheng, Murong Li, Identification of Young's modulus and equivalent spring constraint boundary conditions of the soft tissue with locally observed displacements for endoscopic liver surgery, *Comput. Methods Biomech. Biomed. Eng.* 25 (4) (2022) 439–454.
- [21] Daniel Rueckert, Luke I. Sonoda, Carmel Hayes, Derek L.G. Hill, Martin O. Leach, David J. Hawkes, Nonrigid registration using free-form deformations: application to breast MR images, *IEEE Trans. Med. Imaging* 18 (8) (1999) 712–721.
- [22] Wen-Chi Christina Lee, Mitchell E. Tublin, Brian E. Chapman, Registration of MR and CT images of the liver: comparison of voxel similarity and surface based registration algorithms, *Comput. Methods Programs Biomed.* 78 (2) (2005) 101–114.
- [23] Panlong Xu, Chao Chen, Xinyi Wang, Wentao Li, Jianqi Sun, ROI-based intraoperative MR-CT registration for image-guided multimode tumor ablation therapy in hepatic malignant tumors, *IEEE Access* 8 (2020) 13613–13619.
- [24] Wei Wei, Xu Haishan, Julian Alpers, Marko Rak, Christian Hansen, A deep learning approach for 2D ultrasound and 3D CT/MR image registration in liver tumor ablation, *Comput. Methods Programs Biomed.* 206 (2021) 106117.
- [25] Ha Manh Luu, Wiro Niessen, Theo Van Walsum, Camiel Klink, Adriaan Moelker, An automatic registration method for pre-and post-interventional CT images for assessing treatment success in liver RFA treatment, *Med. Phys.* 42 (9) (2015) 5559–5567.
- [26] Eldad Haber, Jan Modersitzki, Numerical methods for volume preserving image registration, *Inverse Problems* 20 (5) (2004) 1621.
- [27] Andrea Mendizabal, Eleonora Tagliabue, Diego Dall'Alba, Intraoperative estimation of liver boundary conditions from multiple partial surfaces, *Int. J. Comput. Assist. Radiol. Surg.* 18 (7) (2023) 1295–1302.
- [28] Guillaume Mestdagh, Stéphane Cotin, An optimal control problem for elastic registration and force estimation in augmented surgery, in: *International Conference on Medical Image Computing and Computer-Assisted Intervention*, Springer, 2022, pp. 74–83.
- [29] Sergei Nikolaev, Stéphane Cotin, Estimation of boundary conditions for patient-specific liver simulation during augmented surgery, *Int. J. Comput. Assist. Radiol. Surg.* 15 (2020) 1107–1115.
- [30] Tian Xu, Zhen Wang, Yingda Hu, Shilun Du, Ao Du, Zhenyang Yu, Yong Lei, A FEM-based direct method for identification of Young's modulus and boundary conditions in three-dimensional linear elasticity from local observation, *Int. J. Mech. Sci.* 237 (2023) 107797.
- [31] David M. Cash, Michael I. Miga, Tuhin K. Sinha, Robert L. Galloway, William C. Chapman, Compensating for intraoperative soft-tissue deformations using incomplete surface data and finite elements, *IEEE Trans. Med. Imaging* 24 (11) (2005) 1479–1491.
- [32] Jon S. Heiselman, Michael I. Miga, The image-to-physical liver registration sparse data challenge: characterizing inverse biomechanical model resolution, in: *Medical Imaging 2020: Image-Guided Procedures, Robotic Interventions, and Modeling*, vol. 11315, SPIE, 2020, pp. 371–377.
- [33] Jon S. Heiselman, William R. Jarnagin, Michael I. Miga, Intraoperative correction of liver deformation using sparse surface and vascular features via linearized iterative boundary reconstruction, *IEEE Trans. Med. Imaging* 39 (6) (2020) 2223–2234.
- [34] E. Lee Brewer, Logan W. Clements, Jarrod A. Collins, Derek J. Doss, Jon S. Heiselman, Michael I. Miga, Chris D. Pavas, Edward H. Wisdom III, The image-to-physical liver registration sparse data challenge, in: *Medical Imaging 2019: Image-Guided Procedures, Robotic Interventions, and Modeling*, vol. 10951, SPIE, 2019, pp. 364–370.
- [35] Joao Ramalinho, Henry F.J. Tregidgo, Kurinchi Gurusamy, David J. Hawkes, Brian Davidson, Matthew J. Clarkson, Registration of untracked 2D laparoscopic ultrasound to CT images of the liver using multi-labelled content-based image retrieval, *IEEE Trans. Med. Imaging* 40 (3) (2020) 1042–1054.

- [36] Longfei Ma, Hanying Liang, Boxuan Han, Shizhong Yang, Xinran Zhang, Hongen Liao, Augmented reality navigation with ultrasound-assisted point cloud registration for percutaneous ablation of liver tumors, *Int. J. Comput. Assist. Radiol. Surg.* 17 (9) (2022) 1543–1552.
- [37] Shuwei Xing, Derek W. Cool, Lori Gardi, Jeffrey Bax, Elvis C.S. Chen, Terry M. Peters, Aaron Fenster, A 2D/3D US/CT-guided system for percutaneous focal liver thermal ablation, in: *Medical Imaging 2022: Image-Guided Procedures, Robotic Interventions, and Modeling*, vol. 12034, SPIE, 2022, pp. 237–245.
- [38] Jane M. Blackall, Graeme P. Penney, Andrew P. King, Andreas N. Adam, David J. Hawkes, Tracking alignment of sparse ultrasound with preoperative images of the liver and an interventional plan using models of respiratory motion and deformation, in: *Medical Imaging 2004: Visualization, Image-Guided Procedures, and Display*, vol. 5367, SPIE, 2004, pp. 218–227.
- [39] Wolfgang Wein, Shelby Brunke, Ali Khamene, Matthew R. Callstrom, Nassir Navab, Automatic CT-ultrasound registration for diagnostic imaging and image-guided intervention, *Med. Image Anal.* 12 (5) (2008) 577–585.
- [40] Jaime Garcia Guevara, Igor Peterlik, Marie-Odile Berger, Stephane Cotin, Biomechanics-based graph matching for augmented CT-CBCT, *Int. J. Comput. Assist. Radiol. Surg.* 13 (2018) 805–813.
- [41] Stefano Moriconi, Maria A. Zuluaga, H. Rolf Jäger, Parashkev Nachev, Sébastien Ourselin, M. Jorge Cardoso, Elastic registration of geodesic vascular graphs, in: *Medical Image Computing and Computer Assisted Intervention–MICCAI 2018: 21st International Conference, Granada, Spain, September 16–20, 2018, Proceedings, Part I*, Springer, 2018, pp. 810–818.
- [42] Hui Xue, Christina Malamateniou, Joanna Allsop, Latha Srinivasan, Joseph V. Hajnal, Daniel Rueckert, Automatic extraction and matching of neonatal cerebral vasculature, in: *3rd IEEE International Symposium on Biomedical Imaging: Nano to Macro, 2006, IEEE, 2006*, pp. 125–128.
- [43] F. Nazem, Alireza Ahmadian, N. Dadashi Seraj, Masoomeh Giti, Two-stage point-based registration method between ultrasound and CT imaging of the liver based on ICP and unscented Kalman filter: a phantom study, *Int. J. Comput. Assist. Radiol. Surg.* 9 (2014) 39–48.
- [44] Chaity Biswas, Rehena Nasrin, Muhammad S. Ahmad, Numerical analogy of bioheat transfer and microwave cancer therapy for liver tissue, *Heat Transf.* 51 (7) (2022) 6403–6430.
- [45] Christopher P. Lee, Zhoubing Xu, Ryan P. Burke, Rebecca B. Baucom, Benjamin K. Poulouse, Richard G. Abramson, Bennett A. Landman, Evaluation of five image registration tools for abdominal CT: pitfalls and opportunities with soft anatomy, in: *Proceedings of Spie—the International Society for Optical Engineering*, vol. 9413, NIH Public Access, 2015.
- [46] Eduard Serradell, Miguel Amável Pinheiro, Raphael Sznitman, Jan Kybic, Francesc Moreno-Noguer, Pascal Fua, Non-rigid graph registration using active testing search, *IEEE Trans. Pattern Anal. Mach. Intell.* 37 (3) (2014) 625–638.
- [47] Delia Lorente, Francisco Martínez-Martínez, María José Rupérez, Miguel A. Lago, Marcelino Martínez-Sober, Pablo Escandell-Montero, José María Martínez-Martínez, Sandra Martínez-Sanchis, Antonio J. Serrano-López, C. Monserrat, et al., A framework for modelling the biomechanical behaviour of the human liver during breathing in real time using machine learning, *Expert Syst. Appl.* 71 (2017) 342–357.
- [48] Matthieu Nesme, Yohan Payan, François Faure, Efficient, physically plausible finite elements, in: *Eurographics*, 2005.
- [49] You Zhang, Michael R. Folkert, Xiaokun Huang, Lei Ren, Jeffrey Meyer, Joubin Nasehi Tehrani, Robert Reynolds, Jing Wang, Enhancing liver tumor localization accuracy by prior-knowledge-guided motion modeling and a biomechanical model, *Quant. Imaging Med. Surg.* 9 (7) (2019) 1337.
- [50] Chang-Min Lee, Min-Young Jeong, Sam-Youl Yoon, Laparoscopic liver resection enhanced by an intervention-guided fluorescence imaging technique using sodium fluorescein, *J. Clin. Med.* 10 (16) (2021) 3663.
- [51] Hui Jun Lim, Adrian Kah Heng Chiow, Lip Seng Lee, Siong San Tan, Brian K.P. Goh, Ye Xin Koh, Chung Yip Chan, Ser Yee Lee, Novel method of intraoperative liver tumour localisation with indocyanine green and near-infrared imaging, *Singapore Med. J.* 62 (4) (2021) 182.
- [52] Yoshinobu Shimohigashi, Ryo Toya, Tetsuo Saito, Osamu Ikeda, Masato Maruyama, Keisuke Yonemura, Yuji Nakaguchi, Yudai Kai, Yasuyuki Yamashita, Natsuo Oya, et al., Tumor motion changes in stereotactic body radiotherapy for liver tumors: an evaluation based on four-dimensional cone-beam computed tomography and fiducial markers, *Radiat. Oncol.* 12 (2017) 1–8.
- [53] Jennifer Dhont, Jef Vandemeulebroucke, Manuela Burghilea, Kenneth Poels, Tom Depuydt, Robbe Van Den Begin, Cyril Jaudet, Christine Collen, Benedikt Engels, Truus Reynders, et al., The long-and short-term variability of breathing induced tumor motion in lung and liver over the course of a radiotherapy treatment, *Radiother. Oncol.* 126 (2) (2018) 339–346.
- [54] Hua-Chieh Shao, Jing Wang, Ti Bai, Jaehee Chun, Justin C. Park, Steve Jiang, You Zhang, Real-time liver tumor localization via a single X-ray projection using deep graph neural network-assisted biomechanical modeling, *Phys. Med. Biol.* 67 (11) (2022) 115009.
- [55] Anil Gupta, Rishabh Kumar, Hanuman Prasad Yadav, Manik Sharma, Rose Kamal, Deepak Thaper, Prabir Banik, Shipra Gupta, Kartik Saroha, Sandeep Singh, et al., Feasibility of 4D CT simulation with synchronized intravenous contrast injection in hepatocellular carcinoma, *Rep. Pr. Oncol. Radiother.* 25 (2) (2020) 293–298.